Polymer Journal (2021) 53:895–905
https://doi.org/10.1038/s41428-021-00492-0

ORIGINAL ARTICLE

Confined crystallization and chain conformational change in electrospun poly(ethylene oxide) nanofibers

Nhu Quynh Nguyen[1] · Ting-Fang Chen[1] · Chieh-Tsung Lo[1]

Received: 5 March 2021 / Revised: 1 April 2021 / Accepted: 4 April 2021 / Published online: 12 May 2021
© The Society of Polymer Science, Japan 2021

Abstract

This study focused on understanding the confined crystallization of poly(ethylene oxide) (PEO) in electrospun nanofibers. The effect of thermal treatment on PEO crystallization was also studied. An electrospinning process with a rotating drum collector enabled stretching and aligning of polymer chains, which resulted in the formation of a planar zigzag conformation. The confined environment in nanofibers facilitated an ordered crystal arrangement, resulting in an increase in the degree of crystallinity with a decrease in the fiber diameter. By contrast, large fibers extended solvent evaporation, which resulted in large crystallite sizes. The confined geometry and mechanical force provided by a rotating collector induced the preferred crystal orientation parallel to the fiber axis. Upon thermal annealing, the stretched PEO chains relaxed, resulting in a change from the metastable zigzag conformation to a stable helical conformation. Thermal treatment monotonically increased the melting temperature, degree of crystallinity, and crystallite size of PEO nanofibers regardless of the fiber diameter but did not influence the orientation of the organized crystals.

Introduction

Polymers with nanoconfined geometries have attracted considerable research attention because of their unique properties. The kinetics and mechanism of the confined crystallization of polymers are particularly crucial because the performances and applications of polymeric materials strongly depend on their crystallization behaviors. Studies have demonstrated polymer crystallization within one-dimensional (1D), two-dimensional (2D), and three-dimensional (3D) confined spaces and have proposed model systems such as polymer ultrathin films prepared through spin coating [1, 2], multilayer films with two distinct alternating polymers produced through coextrusion [3–5], polymers confined in organic or inorganic templates [6, 7], and microphase-separated block copolymers composed of a crystallizable block [8–12]. In contrast to heterogeneous nucleation, which occurs in bulk polymers, polymer crystallization within confined spaces is typically initiated through homogeneous nucleation because of small quantities of heterogeneous nuclei in the nanospace. Homogeneous nucleation substantially reduces the onset crystallization temperature. By contrast, the surface-induction effect resulting from confined surfaces may induce heterogeneous nucleation, which leads to an increase in the onset crystallization temperature. Studies have revealed the effects of confinement on the molecular dynamics, crystal structure, and crystal orientation of semicrystalline polymers. When the size of confined spaces decreases (i.e., polymer chains are more confined), chain mobility reduces. The kinetic effect reduces the crystallization rate and crystallinity. In addition, geometrical restrictions cause a truncation of growing spherulites at the polymer surface, leading to a loss of isotropic spherulitic morphology. Furthermore, the confinement of a polymer during crystallization facilitates the development of oriented lamellar crystals in a direction either perpendicular or parallel to the confined surface planes. These distinctive orientations can be manipulated using the crystallization temperature, size of the confined space, and polymer–surface interaction [13, 14].

Studies have used electrospun nanofibers as a platform to investigate the confined crystallization of semicrystalline polymers [15–30]. Electrospinning is a highly versatile and simple technique for producing fibers with diameters ranging from a few micrometers to tens of nanometers as well

✉ Chieh-Tsung Lo
tsunglo@mail.ncku.edu.tw

[1] Department of Chemical Engineering, National Cheng Kung University, No. 1, University Road, Tainan City 701, Taiwan, ROC

as high surface area-to-volume ratios. Fiber diameters fabricated through electrospinning are approximately two to three orders of magnitude smaller than those fabricated using other techniques, such as drawing and melt spinning [31]. The diameter of electrospun fibers depends on the interplay between variables such as the characteristics of polymer solutions (viscosity, conductivity, surface tension, and concentration), processing parameters (applied voltage, flow rate, and tip-to-collector distance), and spinning environments (humidity and temperature). Over the past decades, various polymer fibers have been produced through electrospinning, and the crystallization and chain orientation within electrospun fibers have been carefully examined [17, 18, 22, 23, 30]. The geometrical confinement spaces of nanofibers typically facilitate polymer chains to extend and align along the fiber axis. In addition, the confinement size influences the crystal orientation, chain mobility, and relaxation behavior. However, other parameters, such as the saturation temperature of the solvent used for electrospinning, thermal or solvent annealing conditions, and collector type, considerably affect the crystallization of electrospun polymer fibers, and the crystallization behavior differs depending on the specific system used for producing fibers.

In this study, we focused on the crystal structure and molecular orientation of poly(ethylene oxide) (PEO) confined in electrospun nanofibers. PEO molecules tend to form a 7/2 helical conformation (*trans–trans–gauche*) and crystallize in a four-chain monoclinic unit cell [15]. However, processing parameters, such as mechanical stretching, solvent evaporation rates, and thermal treatment, may alter the chain conformation of PEO molecules. For example, when PEO is under tension, PEO molecules adopt the planar zigzag conformation (*trans–trans–trans*) [32]. When tension is released, the metastable molecular structure returns to the 7/2 helical conformation [33]. Kakade et al. demonstrated a technique using two electrically charged aluminum plates as a collector to generate aligned electrospun PEO fibers [15]. PEO chains in both the aligned fibers and randomly oriented fibers exhibited the 7/2 helical conformation. Gazzano et al. suggested that PEO crystallization in confined nanofibers resulted in a fibrillar structure rather than the lamellar morphology that is conventionally observed when polymers crystallize in bulk [25]. Song et al. investigated the effect of solvents used in precursor solutions on the crystal structure and thermal properties of electrospun PEO fibers [29]. The high evaporation rate of ethanol in the precursor solution reduced the molecular chain orientation and degree of crystallinity. Although these studies have demonstrated that PEO crystallization within confined spaces affects its microstructure and molecular orientation, studies of the correlation between the confinement size and crystallization behavior of PEO are not comprehensive. Moreover, limited studies have been conducted on crystal structure development and molecular orientation during thermal annealing. The data provided in this study can complement the literature and provide insights into the confined crystallization of PEO in nanofibers.

Experimental

Electrospun nanofiber preparation

PEO with a weight-averaged molecular weight of 600,000 g/mol (Sigma-Aldrich Co.) was dissolved in deionized water under vigorous stirring for 24 h. The PEO solution was loaded in a glass syringe, which was mounted with a syringe pump (KDS 100, KD Scientific). Conventional single-nozzle electrospinning was performed at room temperature by using a power supply (You-Shang Technical Corporation). A rotating drum was used as a collector. We varied the electrospinning parameters, including the concentration of the PEO solution, applied voltage, distance between the needle tip and collector, flow rate, and drum rotating speed, to prepare aligned and uniform PEO nanofibers. After electrospinning, fibers were dried in the air. Subsequently, the samples were annealed at temperatures of 40 and 50 °C in a vacuum oven for 1 day.

Characterization

The morphology of the electrospun PEO nanofibers was observed on a Hitachi SU8010 scanning electron microscope, operated at an accelerating voltage of 10 kV. Before scanning electron microscopy (SEM) was performed, fibers were sputter-coated with gold for 200 s. The diameter and orientation of fibers were analyzed on ImageJ and OrientationJ software, respectively. Fourier transform infrared (FTIR) spectra of PEO nanofibers were obtained at room temperature using a Nicolet 6700 FTIR spectrometer. Differential scanning calorimetry (DSC) was conducted on a Netzsch DSC 200 F3 calorimeter to characterize the thermal and crystallization properties of PEO nanofibers. Samples of 2–5 mg were sealed in aluminum pans. Subsequently, DSC was performed using a heating process from 30 to 90 °C at a heating rate of 5 °C/min. The degree of crystallinity, X_c, was calculated using the following equation:

$$X_c = \frac{\Delta H_m}{\Delta H_m^o} \quad (1)$$

where ΔH_m is the endothermic heat of fusion of the studied sample and ΔH_m^o is the endothermic heat of fusion of the 100% crystalline polymer, which is taken as 203 J/g for PEO [34].

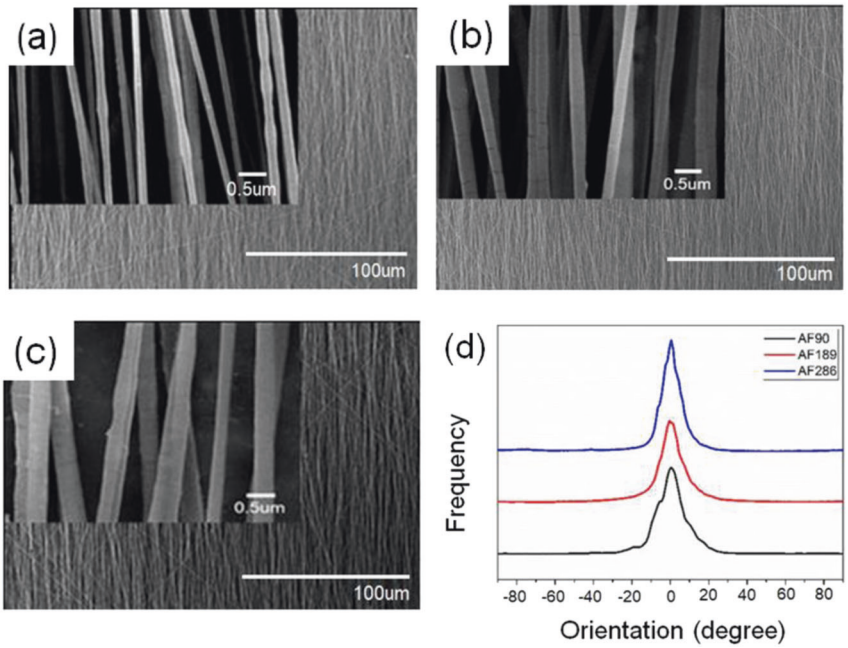

Fig. 1 SEM micrographs of electrospun PEO nanofibers fabricated under various processing conditions. **a** Precursor concentration of 6.0 wt%, needle-to-collector distance of 18 cm, and applied voltage of 15 kV; **b** precursor concentration of 7.5 wt%, needle-to-collector distance of 15 cm, and applied voltage of 18 kV; **c** precursor concentration of 8.0 wt%, needle-to-collector distance of 18 cm, and applied voltage of 15 kV. The flow rate and drum rotating speed were maintained at 0.5 mL/min and 3500 rpm, respectively. **d** Orientation of various electrospun PEO nanofibers

Wide-angle X-ray scattering characterization and analysis

The crystal structure and molecular orientation of electrospun PEO nanofibers were determined through wide-angle X-ray scattering (WAXS), which was performed in Sector BL17A1 at the National Synchrotron Radiation Research Center of Taiwan. The wavelength of the X-ray beam was 1.33 Å.

Herman's orientation function (f) was used to determine the molecular orientation in nanofibers. The f value was calculated using the azimuthal profile obtained from the obtained WAXS patterns as follows [35]:

$$<\cos^2\varphi> = \frac{\sum_0^{\pi/2} I(\varphi)\sin\varphi\cos^2\varphi}{\sum_0^{\pi/2} I(\varphi)\sin\varphi} \quad (2)$$

$$f = \frac{3<\cos^2\varphi> - 1}{2} \quad (3)$$

where φ is the azimuthal angle, $<\cos^2\varphi>$ is a square averaged cosine of the angle φ between the fiber axis and the crystallographic axis, and $I(\varphi)$ is the intensity distribution of a specific crystal plane on the Debye–Scherrer ring. The f value of 1 indicates that crystals exhibit a unified orientation parallel to the fiber axis. By contrast, $f = -0.5$ when polymer chains lie in a plane perpendicular to the fiber axis. The f value approaches 0 when crystals in fibers are randomly oriented.

The crystallite size of the samples was derived from azimuthally averaged 1D WAXS profiles using the following Scherrer equation:

$$\tau = \frac{K}{\beta\cos\theta} \quad (4)$$

where τ is the mean crystallite size obtained from the reflection plane, K is a dimensionless shape factor with a constant value of 0.9, λ is the wavelength of the incident X-ray beam, β is the full width at a half of the maximum intensity, and θ is the half-scattering angle.

Small-angle X-ray scattering characterization and analysis

Small-angle X-ray scattering (SAXS) was conducted in Sector BL23A1 at the National Synchrotron Radiation Research Center of Taiwan and using a Bruker diffractometer (NanoSTAR U System, Bruker AXS Gmbh, Karlsruhe, Germany). The wavelengths of the X-ray beam were 0.54 and 1.54 Å for the synchrotron and in-house X-ray instruments, respectively. Samples were measured at room temperature with a sample-to-detector distance of 2 m. The 2D pattern was azimuthally averaged to obtain the 1D intensity profile (I), which was expressed as a function of the scattering vector, q, where $q = (4\pi\sin\theta)/\lambda$.

Results and discussion

Figure 1 displays the electrospun PEO nanofibers fabricated using various electrospinning conditions. All fibers were

approximately stretched and aligned along the drum rotating direction without the occurrence of beads. During electrospinning, when a polymer solution in a syringe flows through a needle, shear force acts on the polymer solution. Subsequently, the polymer jet is elongated and accelerated under an electric field, thus providing a Columbic force to the jet. Finally, a rotating drum collector exerts a tensile force. The combined first two forces result in chain orientation and stretching, and the tensile force facilitates fiber alignment. The balances between the three forces result in the uniform fibers with a preferred orientation. In this study, we manipulated fiber diameters by varying the precursor concentration, needle-to-collector distance, and applied voltage. The flow rate and drum rotating speed for all samples were maintained at 0.5 mL/min and 3500 rpm, respectively. The resulting mean fiber diameters were 90 ± 9, 189 ± 20, and 286 ± 29 nm. Although several processing conditions were changed, the major parameter influencing the fiber diameters was the precursor concentration. The fiber diameter monotonically increased with an increase in the precursor concentration from 6 wt% to 8 wt%. We designated these nanofibers as AF90, AF189, and AF286.

Figure 1d illustrates the orientation angle of PEO nanofibers along the drum rotating direction. The orientation angles of all samples exhibited a maximum at ~0°, indicating that most of the nanofibers collected on the drum collector exhibited the preferred orientation (along the rolling direction). However, some randomly aligned fibers were observed. During electrospinning, fibers were charged through the applied voltage. The surface charges on fibers repelled neighboring fibers, which allowed fibers to align and separate when fibers were collected on a rotating drum collector in a short collection time. After a long collection time, the accumulated fibers on the collector provided additional repelling force, which caused fibers to deviate from the rolling direction [16]. However, the quantity of randomly aligned fibers was low.

Figure 2 illustrates the DSC curves of the as-prepared electrospun PEO nanofibers. The DSC profile of the solution-cast PEO film with a thickness of approximately 100 µm (assigned as BulkS) is included in the figure for comparison. The endothermic peaks of the PEO nanofibers and solution-cast film were highly asymmetric, and the endothermic peaks were composed of a maximum at a high temperature and a shoulder at a low temperature. The melting temperature of semicrystalline polymers strongly depends on the lamellar thickness of folded chains, and a large lamellar thickness resulted in a high melting temperature. The presence of a maximum and a shoulder indicated that the distribution of the lamellar thickness of folded chains was nonuniform, and at least two types of folded chains formed. The folded chains with a smaller lamellar thickness contributed to a lower melting

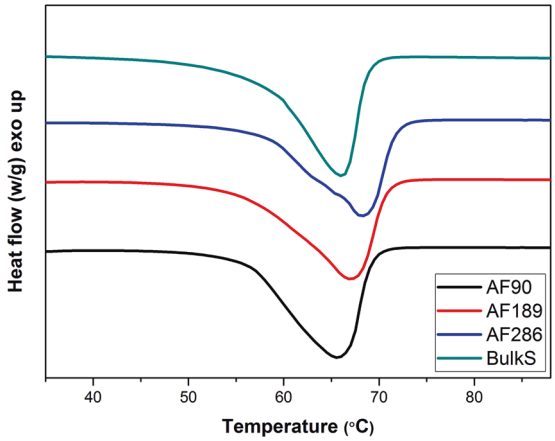

Fig. 2 DSC curves of various as-prepared PEO samples

temperature, whereas the folded chains with a larger lamellar thickness resulted in a higher melting temperature. The nonuniform lamellar thickness was attributed to various crystallization durations in the sample. For the PEO nanofibers and solution-cast film, crystallization occurred during the removal of water. In the fiber and film, water molecules diffused from the inner part of the fiber and film to the surface. Once water was removed, crystallization nearly stopped because of low chain mobility. Therefore, PEO chains close to the surface exhibited longer time for crystallization than PEO chains in the inner part of the fiber and film. Consequently, PEO chains at the surface exhibited a larger lamellar thickness than PEO chains at the inner part of the samples. These results suggested that the fractionated crystallization of the solution-cast film and electrospun fibers was mainly caused by solvent evaporation. Furthermore, the degree of crystallinity of all samples obtained from DSC was between 60% and 70%. A study reported the thermal and crystallization properties of electrospun PEO nanofibers that were prepared in mixed PEO/ethanol solutions [29]. With similar fiber diameters, the degree of crystallinity of PEO nanofibers in that study was consistently lower than that of PEO nanofibers in the present study because ethanol evaporates more rapidly than water. This result confirmed that the high degree of crystallinity of the PEO nanofibers obtained in this study was caused by the slow evaporation of water, which allowed crystals to grow before complete solidification of PEO.

Table 1 summarizes the melting temperature and degree of crystallinity of all samples derived from endothermic profiles at various annealing conditions. Both the melting temperature and degree of crystallinity of all samples increased with an increase in the annealing temperature. However, the changes in the melting temperature and crystallinity were small. This result was associated with the low annealing temperature and the high molecular weight of PEO. As mentioned previously, some crystals formed

during the water removal process. The subsequent annealing mainly induced crystal growth on the existing crystals, resulting in an increase in the crystallite size and lamellar thickness. Because of the low annealing temperatures, chain mobility was slow. In addition, the entanglement of the high-molecular-weight PEO hindered chain movement. Consequently, the melting temperature and degree of crystallinity were not strongly correlated to the annealing temperature. A comparison of the melting temperature and degree of crystallinity of PEO fibers with various fiber diameters indicated that the melting temperature increased, whereas the degree of crystallinity decreased with an increase in the fiber diameter at all annealing conditions. These results indicated that the diameter of PEO nanofibers exhibited a considerable effect on the crystallization behavior of PEO. The increase in the melting temperature with the increase in the fiber diameter was because a large fiber diameter provided more space for crystal growth, which led to thick crystal lamellae. By contrast, when the fiber diameter was small, the confined environment facilitated an ordered arrangement of crystals, resulting in a high degree of crystallinity. Furthermore, the size-dependent crystallinity was associated with the concentration of the precursor solution during fiber fabrication. A high polymer concentration exhibited a high viscosity, which blocked the flow of the solution jet and hindered chain extension during the electrospinning process. By contrast, the polymer chains in the dilute solution exhibited high mobility, enabling the chains to align along the fiber axis during electrospinning, which promoted a high degree of crystallinity. Consequently, a small fiber diameter produced at a low polymer concentration resulted in a high degree of crystallinity, and a large fiber diameter obtained with a high polymer concentration exhibited a low degree of crystallinity.

The FTIR spectra of the various as-prepared PEO samples are displayed in Fig. 3a. In the spectra of all samples, the absorbance at wavenumbers of 1360 and 1343 cm^{-1} resulted from CH_2 wagging; the absorbance at wavenumbers of 960

Table 1 Thermal properties of various PEO samples

Sample	As-prepared		Annealed at 40 °C		Annealed at 50 °C	
	T_m (°C)	Degree of crystallinity (%)	T_m (°C)	Degree of crystallinity (%)	T_m (°C)	Degree of crystallinity (%)
AF90	66.2	66.2	68.0	70.4	68.6	73.2
AF189	67.0	65.4	69.0	68.8	70.0	70.6
AF286	68.8	60.8	69.6	67.1	71.5	69.8
BulkS	66.1	66.9	67.5	68.5	71.1	70.1

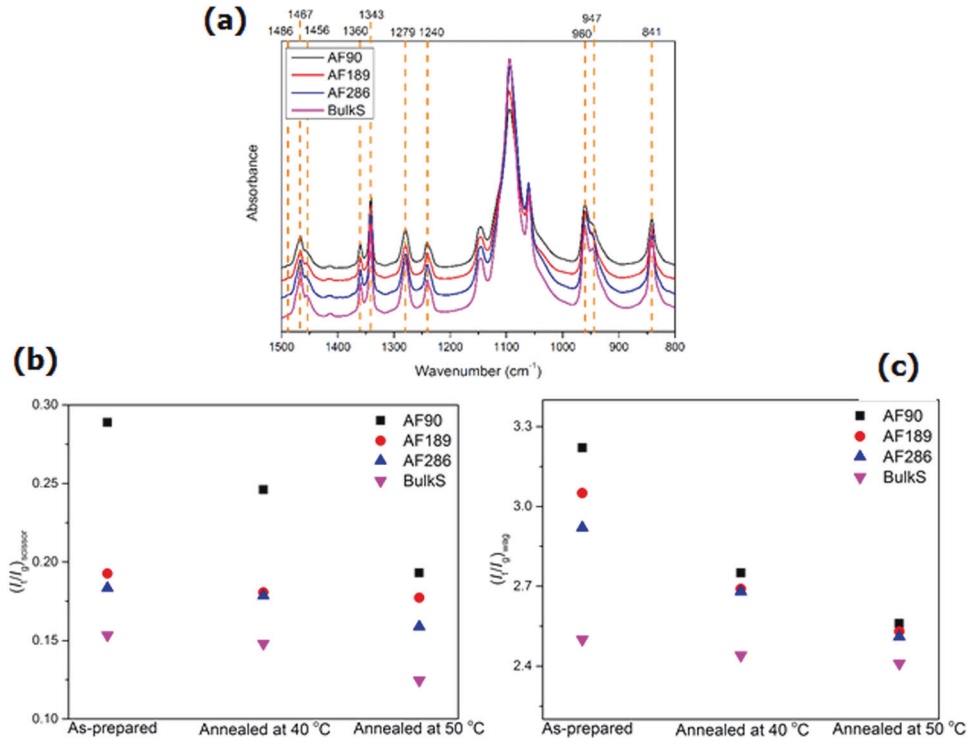

Fig. 3 **a** FTIR spectra of various as-prepared PEO samples; **b** the relative intensities of the 1486 and 1456 cm^{-1} bands; and **c** the relative intensities of the 1343 and 1360 cm^{-1} bands

and 947 cm^{-1} was related to CH_2 rocking; the absorbance at a wavenumber of 841 cm^{-1} was attributed to CH_2 rocking and COC deformation [36]; and the absorbance at wavenumbers of 1279 and 1240 cm^{-1} resulted from CH_2 twisting [37]. Regarding the chain conformation of PEO confined in various geometries, reports have suggested that the absorbance at a wavenumber of 1456 cm^{-1} was associated with *gauche* CH_2 scissor motion [36]. By contrast, the absorbance at a wavenumber of 1486 cm^{-1} corresponded to the *trans* CH_2 scissor motion. The absorbance at a wavenumber of 1467 cm^{-1} was associated with both *trans* and *gauche* CH_2 scissoring [37]. We deconvoluted the absorbance associated with CH_2 scissor motion into three contributions. Figure 3b presents a comparison of the relative areas of the 1486 and 1456 cm^{-1} bands in the FTIR spectra of the various samples ($(I_t/I_g)_{scissor}$). These values qualitatively indicated the relative amounts of *trans* and *gauche* conformations of PEO chains in the samples under various processing conditions [36]. The $(I_t/I_g)_{scissor}$ values for the PEO chains confined in a fibrous morphology were considerably higher than those for the PEO chains in the film. Moreover, the $(I_t/I_g)_{scissor}$ values decreased with an increase in the fiber diameter. This result indicated that the geometry of the confinement facilitated the occurrence of the *trans* conformation, which led to the zigzag conformation. Furthermore, as-prepared samples exhibited higher $(I_t/I_g)_{scissor}$ values. Thermal treatment caused a decrease in the $(I_t/I_g)_{scissor}$ values, and a high annealing temperature resulted in lower $(I_t/I_g)_{scissor}$ values. Thermal treatment induced relaxation of stretched PEO chains, resulting in the conformational change from the metastable zigzag conformation to the stable helical conformation. Therefore, the *trans* conformation decreased, whereas the *gauche* conformation increased when the annealing temperature increased. Furthermore, a study suggested the use of the CH_2 wag motion at wavenumbers of 1343 and 1360 cm^{-1}, which corresponded to the zigzag and helical conformations, respectively, to determine the relative contents of the conformations in electrospun fibers because other aforementioned absorbance may contain two conformational modifications [38]. Figure 3c presents a comparison of the relative areas of the 1343 and 1360 cm^{-1} bands in the FTIR spectra of the various samples ($(I_t/I_g)_{wag}$). The variations in the $(I_t/I_g)_{wag}$ values agree well with those in the $(I_t/I_g)_{scissor}$ values. Decreasing the fiber diameter preferentially produced the zigzag conformation. Thermal treatment relaxed the stretched chains, resulting in an increase in the content of the helical conformation. However, the presence of the zigzag conformation in electrospun PEO nanofibers was inconsistent with the results in a previous study [15]. In that study, aligned PEO nanofibers with diameters of 100–400 nm were prepared through electrospinning in a PEO/water solution. The oriented fibers only exhibited the helical conformation. We speculated that the absence of the zigzag conformation was because the fibers were collected using a flat plate collector. Although the flat plate collector enabled the production of uniaxially aligned fibers, inadequate mechanical drawing prevented chains from stretching. By contrast, the mechanical drawing provided by the rotating drum in the present study caused chain stretching, resulting in the formation of the zigzag conformation.

The increase in the *trans* conformation in the PEO fibers was attributed to several electrospinning processes. When PEO chains in the precursor solution passed through the spinneret under the applied voltage, the shear force and Columbic force resulted in elongated and highly oriented polymer chains. Although the bending instability during jet formation caused the randomization of oriented chains, the tensile force exercised by the rotating drum collector overcame the bending instability, resulting in oriented polymer chains confined in oriented fibers. In addition to the orientation of polymer chains, these forces facilitated the polymer chains to adopt the fully extended planar zigzag conformation. However, during solvent evaporation, the highly oriented and stretched chains were relaxed by solvent molecules, which induced conformational transformation from the metastable zigzag conformation to the stable helical conformation. Consequently, zigzag and helical conformations coexisted in the nanofibers.

Figure 4 displays the WAXS patterns of the various PEO samples without thermal treatment. The WAXS pattern of the BulkS sample was composed of two major rings (Fig. 4a). The inner and outer rings corresponded to the (120) and (112)/(032) planes with domain spacings of 4.49 and 3.83 Å, respectively. The presence of the crystal planes was consistent with the monoclinic structure of PEO crystals. The ring pattern suggested that crystals were randomly oriented. By contrast, discrete arcs along the equator were observed in the WAXS patterns of PEO nanofibers, indicating that crystal planes were aligned parallel to the fiber axis of the aligned nanofibers (Fig. 4b–d). However, the differences in crystal orientation between the fibers with various diameters were indistinguishable. Although crystal alignment differed in the film and fibers, the crystal structure was identical for PEO crystallized with and without confinement. Studies have demonstrated the effect of the fiber diameter on crystal orientation [27, 39]. For poly($_L$-lactic acid) (PLLA) and poly(caprolactone) (PCL), preferential crystal orientation was still obtained when fiber diameters reached approximately 2000 and 500 nm, respectively [27]. By contrast, polyethylene (PE) crystals exhibited a high degree of orientation at diameters <200 nm [39]. In this study, the fibers with diameters <300 nm exhibited preferential crystal orientation. The various critical fiber diameters that could maintain preferential crystal orientation were attributed to the chain flexibility of the various polymers, in which rigid chains favored preferential crystal orientation, whereas flexible chains tended to form random crystal orientation [27]. In the various semicrystalline

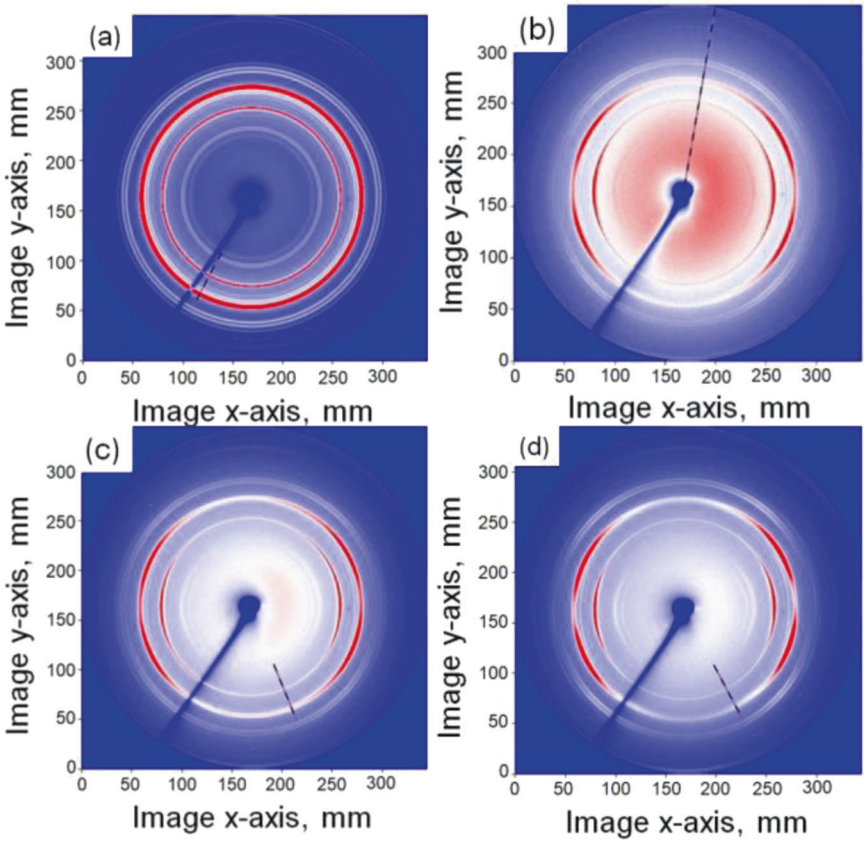

Fig. 4 Two-dimensional WAXS patterns of various as-prepared PEO samples. **a** BulkS, **b** AF90, **c** AF189, and **d** AF286

polymers, the characteristic ratios of PLLA, PCL, PE, and PEO are 11.8 [40], 5.9 [41], 6.8 [42], and 6.9 [43], respectively. The high characteristic ratio of PLLA indicated its rigid chain characteristic, which allowed PLLA crystals to develop in a high degree of orientation. However, although the rest of the three polymers exhibited similar characteristic ratios, the critical fiber diameters varied. Another possible factor that influenced the critical fiber diameter was the solvent used for electrospinning. When the solvent easily evaporated, polymer chains solidified rapidly, which enabled the retention of the stretched conformation. The stretched chain conformation and tightly packed chains facilitated the development of highly oriented crystals. In the aforementioned studies [27, 39], PLLA, PCL, and PE were electrospun using chloroform, 2,2,2-trifluoroethanol, and *p*-xylene as solvents. Notably, PE was electrospun at 112 °C. At such high temperatures, the saturated vapor pressure of *p*-xylene calculated using the Antoine equation was 355 mmHg, which was considerably larger than the saturated vapor pressures of chloroform, 2,2,2-trifluoroethanol, and water. This indicated that *p*-xylene was easily evaporated, and PE nanofibers prepared using *p*-xylene easily retained stretching and alignment. However, this result disagreed with the experimental findings. Therefore, chain flexibility and solvents were not the major parameters influencing crystal orientation. Instead, the most critical parameter was the approach for collecting electrospun nanofibers. In the preparation of PE nanofibers, a flat collector was used [39]. By contrast, a rotating wheel or drum collector was used to fabricate PLLA, PCL, and PEO fibers [27]. The mechanical force provided by the rotating collectors facilitated crystal orientation. Consequently, a high degree of orientation was maintained even when the fiber diameter was large.

The azimuthal intensity profiles of the (120) reflection for all samples are presented in Fig. 5a. The BulkS sample manifested approximately homogeneous azimuthal intensity distributions, which again indicated an absence of a local crystal orientation order. By contrast, the enhanced intensities at an azimuthal angle of approximately 0° for PEO nanofibers were related to the preferential ordering of PEO crystals. We used the Hermans orientation function to determine the crystal orientation in all samples. The Hermans orientation functions of all the PEO samples were calculated according to the azimuthal intensity profiles; the results are summarized in Table 2. The Hermans orientation functions of the BulkS sample at various annealing conditions were between −0.008 and −0.017. The values close to 0 proved that PEO crystals in the solution-cast film were randomly oriented. By contrast, the Hermans orientation functions of the electrospun PEO nanofibers with various

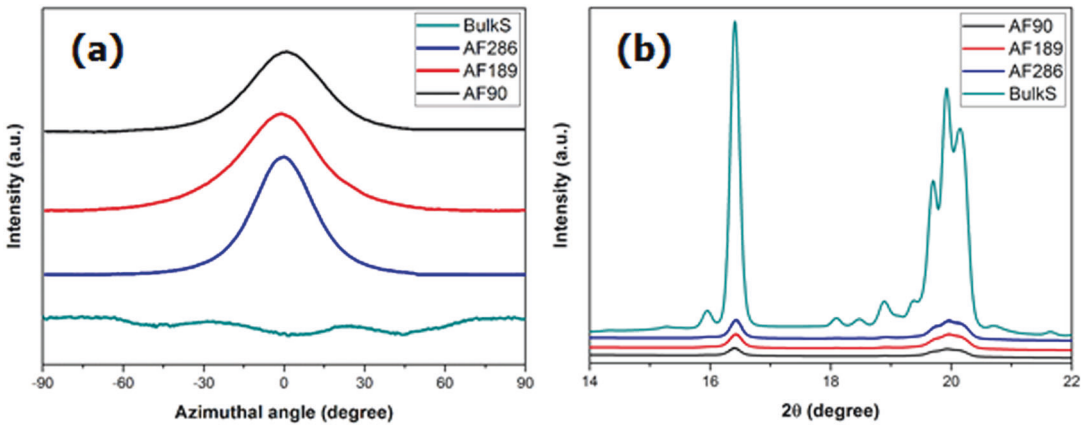

Fig. 5 **a** Azimuthal intensity profiles of the (120) plane of the various as-prepared PEO samples and **b** one-dimensional WAXS patterns of the various as-prepared PEO samples

Table 2 Hermans orientation function of various PEO samples

Sample	As-prepared	Annealed at 40 °C	Annealed at 50 °C
AF90	0.81	0.82	0.75
AF189	0.74	0.86	0.80
AF286	0.80	0.81	0.75
BulkS	−0.017	−0.008	−0.016

Table 3 Peak area ratio of various PEO samples

Sample	As-prepared	Annealed at 40 °C	Annealed at 50 °C
AF90	2.7	2.4	2.4
AF189	2.5	2.6	2.6
AF286	2.7	2.4	2.5
BulkS	2.2	2.1	2.1

fiber diameters and annealing temperatures were approximately 0.8, which is close to 1, suggesting that crystals were preferentially oriented parallel to the fiber axis. The preferred crystal orientation in electrospun PEO nanofibers was attributed to the confined geometry provided by nanofibers, which facilitated the development of densely packed aligned chains. By contrast, crystallization in the solution-cast film was unconfined. Crystal development proceeded in any direction, which resulted in random orientation of crystals. Furthermore, the variation in the Herman's orientation function at various annealing temperatures was not considerable, which indicated that the confined geometry was the major parameter influencing the orientation of PEO crystals.

We converted the 2D WAXS patterns to 1D profiles, as displayed in Fig. 5b. The intensity of the BulkS sample was considerably higher than that of the PEO nanofibers because the quantity of the BulkS sample used for the WAXS measurements was higher than that of the electrospun PEO nanofibers. All samples exhibited strong diffraction peaks at 16.4° and 19.9°, which resulted from the monoclinic structure [44, 45], as indicated in the preceding section. The three major diffraction peaks of PEO molecules with the triclinic structure (zigzag conformation) that occurred at 2θ of 17.7°, 21.0°, and 21.7° were not observed [33]. This result could probably be attributed to the small crystallite size or low quantity of PEO crystals that organized into the triclinic unit cell. Table 3 summarizes the ratio of the-peak area between the (120) and (112)/(032) planes. The peak area ratios were 2.4–2.7 for the PEO fibers, whereas the peak area ratios were approximately 2.1 for the BulkS sample, indicating that crystals preferentially developed along the (120) plane in the PEO fibers more than those did in the BulkS sample. This result agreed well with the crystallization of PEO confined in core-sheath nanofibers [46].

Table 4 presents the crystallite sizes of the various samples calculated from the (120) reflection using the Scherrer equation. The crystallite sizes of the PEO nanofibers were smaller than those of the BulkS sample at various annealing conditions. PEO crystallization in a confined space restricted chain mobility, which hindered crystal growth. Consequently, the crystallite size of PEO in the confined space was smaller than that in the unconfined space. Additionally, the high degree of freedom of polymer chains at the surface facilitated nucleation and crystal growth. The high surface-to-volume ratio in the PEO nanofibers indicated that the number of nuclei per volume was high in the PEO nanofibers, which resulted in a decrease in the mean crystallite size in the PEO nanofibers. Furthermore, the crystallite size varied with the fiber diameter and annealing temperature. The crystallite size increased with an increase in the dimension of the confinement. This increase was associated with the decrease in

Table 4 Crystallite size of various PEO samples

Sample	As-prepared (nm)	Annealed at 40 °C (nm)	Annealed at 50 °C (nm)
AF90	23.3	25.1	27.7
AF189	24.6	25.6	28.3
AF286	27.8	28.5	30.4
BulkS	37.2	37.5	40.5

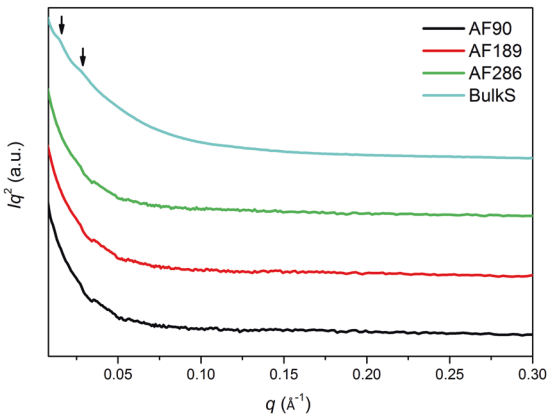

Fig. 6 Kratky plots [$q^2I(q)$ versus q] of the SAXS curves of the various as-prepared PEO samples

the surface-to-volume ratio with increasing fiber diameter. Moreover, high annealing temperatures allowed crystals to grow more rapidly, which increased the crystallite size. Consequently, crystals formed in a less confined space and a high annealing temperature were larger than those formed in a more confined space and a low annealing temperature.

SAXS was performed to analyze the crystal morphology of the PEO samples. As presented in Fig. 6, all the SAXS patterns exhibited strong scattering intensities in the low-q region. This feature indicated the presence of long-range disorder, which resulted from nanovoids existing in the samples [47]. The SAXS profile of the solution-cast film exhibited two discernible peaks. The ratio of the peak position was 1:2, indicating the presence of a lamellar morphology composed of alternate crystal lamellae and amorphous regions. The lamellar thickness and long period of the solution-cast film calculated using the 1D correlation function were 34.1 and 43.0 nm, respectively [48]. Thermal annealing at 40 and 50 °C increased the lamellar thickness to 37.8 and 46.0 nm, respectively, whereas the long period increased to 48.0 and 56.5 nm, respectively. Chain-folded lamella development in solution-cast films is commonly observed when polymers crystallize in bulk. By contrast, the SAXS curves of the PEO nanofibers did not display any discernible peaks. As suggested in the literature [25], when crystallization occurs in nanofibers, chain stretching facilitated crystallization to develop into a fibrillar structure

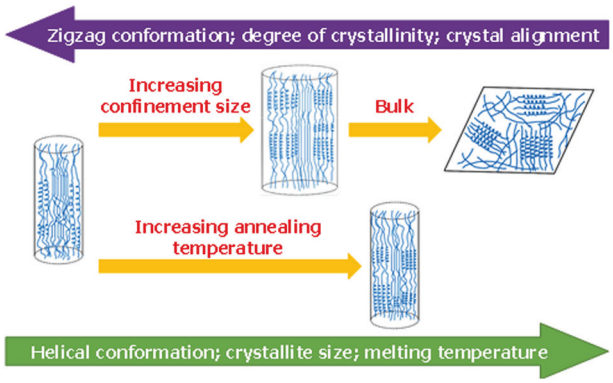

Fig. 7 Schematic of crystal development of PEO in the nanofibers and solution-cast film as functions of the confinement size and annealing temperature

rather than the conventional chain-folded lamellae occurring in bulk polymer. The crystals organized in a fibrillar structure exhibited large size distributions that smeared out the structure factor, which caused the absence of the SAXS peak. Additionally, the stretched polymer chains with preferential chain orientation along the fiber axis increased the electron density of the amorphous phase, which reduced the contrast between the crystal and amorphous phases. Therefore, the SAXS signal contributed by a long-range order was less pronounced. A similar behavior was obtained in electrospun polypropylene nanofibers [47].

Figure 7 presents schematics of crystal development in the nanofibers and solution-cast film as functions of the confinement size and annealing temperature. When the fiber diameters were small, polymer chains were densely packed in the fibers, which formed majorly the zigzag conformation in the inner part of fibers and the helical conformation close to the fiber surface. This was because solvent molecules exhibited longer time to swell the PEO chains close to the surface, which promoted the development of the helical conformation. The densely packed chains facilitated crystal development, and the degree of crystallinity of PEO confined in small fibers was higher than that of PEO confined in large fibers. By contrast, large fibers extended solvent evaporation, resulting in a large crystallite size. PEO crystals confined in the fibers with diameters <300 nm were aligned parallel to the fiber axis. By contrast, PEO crystallization within the solution-cast film developed into an isotropic spherulite structure. Because the polymer chains did not experience any stress, they were not stretched; therefore, they adopted a random walk conformation. After crystallization, the helical conformation was predominant. Additionally, the nonconfined geometry facilitated crystal growth without the preferred orientation, and the crystallite size in the solution-cast PEO film was considerably higher than that in the electrospun fibers. When PEO was subjected to thermal annealing, chain mobility increased, inducing

crystal development. The increase in chain mobility induced the relaxation of PEO chains, which allowed the metastable zigzag conformation to transfer to the stable helical conformation. Furthermore, subsequent thermal annealing mainly resulted in crystal growth from the preexisting crystals without the occurrence of secondary nucleation, leading to an increase in the crystallite size and thickening of the lamellar thickness. This result increased the melting temperature regardless of the sample geometry.

Conclusions

We demonstrated the chain conformation and crystallization behavior of PEO confined in electrospun nanofibers. PEO chains within the nanofibers collected using a rotating drum collector exhibited the preferred orientation along the fiber axis. When the fiber diameter decreased, the confinement facilitated tightly packed chains, resulting in an increase in the degree of crystallinity. Moreover, the PEO chains tended to form a planar zigzag conformation. Increasing the fiber diameter reduced the packing of polymer chains, thereby enabling crystal development. Consequently, the melting temperature and crystallite size increased. When the electrospun nanofibers were subjected to thermal treatment, chain mobility increased and the stretched chains relaxed, which induced changes in the conformation from the zigzag conformation to the 7/2 helical conformation. The conformational change did not alter the crystal orientation. Instead, the melting temperature, degree of crystallinity, and crystallite size monotonically increased with an increase in the annealing temperature.

Acknowledgements This work was financially supported by the Ministry of Science and Technology of Taiwan under Grant Nos. 105-2628-E-006-009-MY3 and 108-2221-E-006-053-MY3. The authors gratefully acknowledge the use of SAXS belonging to the Instrument Center of National Cheng Kung University.

Compliance with ethical standards

Conflict of interest The authors declare no competing interests.

Publisher's note Springer Nature remains neutral with regard to jurisdictional claims in published maps and institutional affiliations.

References

1. Frank CW, Rao V, Despotopoulou MM, Pease RFW, Hinsberg WD, Miller RD, et al. Structure in thin and ultrathin spin-cast polymer films. Science. 1996;273:912–5.
2. Hu ZJ, Huang HY, Zhang FJ, Du BY, He TB. Thickness-dependent molecular chain and lamellar crystal orientation in ultrathin poly(di-n-hexylsilane) films. Langmuir. 2004;20:3271–7.
3. Jin Y, Rogunova M, Hiltner A, Baer E, Nowacki R, Galeski A, et al. Structure of polypropylene crystallized in confined nanolayers. J Polym Sci Polym Phys Ed. 2004;42:3380–96.
4. Wang HP, Kenum JK, Hiltner A, Baer E, Freeman B, Rozanski A, et al. Confined crystallization of polyethylene oxide in nanolayer assemblies. Science. 2009;323:757–60.
5. Orench IP, Stribeck N, Ania F, Baer E, Hiltner A, Calleja FJB. SAXS study on the crystallization of PET under physical confinement in PET/PC multilayered films. Polymer. 2009;50:2680–7.
6. Woo E, Huh J, Jeong YG, Shin K. From homogeneous to heterogeneous nucleation of chain molecules under nanoscopic cylindrical confinement. Phys Rev Lett. 2007;98:136103.
7. Shin K, Woo E, Jeong YG, Kim C, Huh J, Kim KW. Crystalline structures, melting, and crystallization of linear polyethylene in cylindrical nanopores. Macromolecules. 2007;40:6617–23.
8. Rangarajan P, Register RA, Fetters LJ, Bras W, Naylor S, Ryan AJ. Crystallization of a weakly segregated polyolefin diblock copolymer. Macromolecules. 1995;28:4932–8.
9. Ryan AJ, Fairclough JPA, Hamley IW, Mai SM, Booth C. Chain folding in crystallizable block copolymers. Macromolecules. 1997;30:1723–7.
10. Chen HL, Wu JC, Lin TL, Lin JS. Crystallization kinetics in microphase-separated poly(ethylene oxide)-block-poly(1,4-butadiene). Macromolecules. 2001;34:6936–44.
11. Huang P, Zhu L, Guo Y, Ge Q, Jing AJ, Chen WY, et al. Confinement size effect on crystal orientation changes of poly(ethylene oxide) blocks in poly(ethylene oxide)-b-polystyrene diblock copolymers. Macromolecules. 2004;37:3689–98.
12. Chen YW, Yeh BJ, Hashimoto T, Liao SY, Lo CT. Hydrogen bonding induced co-ordering and interfacial curvature controlled crystallization behavior of binary copolymer blends. Macromolecules. 2018;51:7699–712.
13. Zhu L, Cheng SZD, Calhoum BH, Ge Q, Quirk RP, Thomas EL, et al. Crystallization temperature-dependent crystal orientations within nanoscale confined lamellar of a self-assembled crystalline-amorphous diblock copolymer. J Am Chem Soc. 2000;122:5957–67.
14. Carr JM, Langhe DS, Ponting MT, Hiltner A, Baer E. Confined crystallization in polymer nanolayered films: a review. J Mater Res. 2012;27:1326–50.
15. Kakade MV, Givens S, Gardner K, Lee KH, Chase DB, Rabolt JF. Electric field induced orientation of polymer chains in macroscopically aligned electrospun polymer nanofibers. J Am Chem Soc. 2007;129:2777–82.
16. Yee WA, Kotaki M, Liu Y, Lu X. Morphology, polymorphism behavior and molecular orientation of electrospun poly(vinylidene fluoride) fibers. Polymer. 2007;48:512–21.
17. Kongkhlang T, Tashiro K, Kotaki M, Chirachanchai S. Electrospinning as a new technique to control the crystal morphology and molecular orientation of polyoxymethylene nanofibers. J Am Chem Soc. 2008;130:15460–6.
18. Lim CT, Tan EPS, Ng SY. Effects of crystalline morphology on the tensile properties of electrospun polymer nanofibers. Appl Phys Lett. 2008;92:141908.
19. Chan KHK, Wong SY, Li X, Zhang YZ, Lim PC, Lim CT. et al. Effect of molecular orientation on mechanical property of single electrospun fiber of poly[(R)-3-hydroxybutyrate-co-(R)-3-hydroxyvalerate].J Phys Chem B.2009;113:13179–85.
20. Cheng YW, Lu HA, Wang YC, Thierry A, Lotz B, Wang C. Syndiotactic polystyrene nanofibers obtained from high-temperature solution electrospinning process. Macromolecules. 2010;43:2371–6.
21. Kolbuk D, Sajkiewicz P, Kowalewski TA. Optical birefringence and molecular orientation of electrospun polycaprolactone fibers by polarizing-interference microscopy. Eur Polym J. 2012;48:275–83.
22. Ma Q, Pyda M, Mao B, Cebe P. Relationship between the rigid amorphous phase and mesophase in electrospun fibers. Polymer. 2013;54:2544–54.

23. Gong L, Chase DB, Noda I, Liu J, Martin DC, Ni C. et al.Discovery of β-form crystal structure in electrospun poly[(R)-3-hydroxybutyrate-co-(R)-3-hydroxyhexanoate] (PHBHx) nanofibers: from fiber mats to single fibers.Macromolecules. 2015;48:6197–205.
24. Wang C, Fang CY, Wang CY. Electrospun poly(butylene terephthalate) fibers: entanglement density effect on fiber diameter and fiber nucleating ability towards isotactic polypropylene. Polymer. 2015;72:21–9.
25. Gazzano M, Gualandi C, Zucchelli A, Sui T, Korsunsky AM, Reinhard C, et al. Structure-morphology correlation in electrospun fibers of semicrystalline polymers by simultaneous synchrotron SAXS-WAXD. Polymer. 2015;63:154–63.
26. Baqeri M, Abolhasani MM, Mozdianfard MR, Guo Q, Oroumei A, Naebe M. Influence of processing conditions on polymorphic behavior, crystallinity, and morphology of electrospun poly(vinylidene fluoride) nanofibers. J Appl Polym Sci. 2015;132:42304.
27. Liu J, Lin DY, Wei B, Martin DC. Single electrospun PLLA and PCL polymer nanofibers: increased molecular orientation with decreased fiber diameter. Polymer. 2017;118:143–9.
28. Chung J, Chung JW, Priestley RD, Kwak SY. Confinement-induced change in chain topology of ultrathin polymer fibers. Macromolecules. 2018;51:4229–37.
29. Song Z, Chiang SW, Chu X, Du H, Li J, Gan L, et al. Effects of solvent on structures and properties of electrospun poly(ethylene oxide) nanofibers. J Appl Polym Sci. 2018;135:45787.
30. Maurya AK, Weidenbacher L, Spano F, Forunato G, Rossi RM, Frenz M, et al. Structure insights into semicrystalline states of electrospun nanofibers: a multiscale analytical approach. Nanoscale. 2019;11:7176–87.
31. Li D, Xia Y. Electrospinning of nanofibers: reinventing the wheel? Adv Mater. 2004;16:1151–70.
32. Ding Y, Rabolt JF, Chen Y, Olson KL, Baker GL. Studies of chain conformation in triblock oligomers and microblock copolymers of ethylene and ethylene oxide. Macromolecules. 2002;35:3914–20.
33. Takahashi Y, Sumita I, Tadokoro H. Structural studies of polyethers. IX. Planar zigzag modification of poly(ethylene oxide). J Polym Sci Polym Phys Ed. 1973;11:2113–22.
34. Lisowski MS, Liu Q, Cho J, Runt J, Yeh F, Hsiao BS. Crystallization behavior of poly(ethylene oxide) and its blends using time-resolved wide- and small-angle X-ray scattering. Macromolecules. 2000;33:4842–9.
35. Mohamed A, Larbi FBC, Dubault A, Halary JL. Structural study of semi-crystalline blends of poly(vinylidene fluoride) and poly (methyl methacrylate) by means of linear correlation and interface distribution functions. e-Polymers. 2005;5:56.
36. Li X, Hsu SL. An analysis of the crystallization behavior of poly (ethylene oxide)/poly(methyl methacrylate) blends by spectroscopic and calorimetric techniques. J Polym Sci Polym Phys Ed. 1984;22:1331–42.
37. Chrissopoulou K, Andrikopoulos KS, Fotiadou S, Bollas S, Karageorgaki C, Christofilos D, et al. Crystallinity and chain conformation in PEO/layered silicate nanocomposites. Macromolecules. 2011;44:9710–22.
38. Su Z, Li J, Li Q, Ni T, Wei G. Chain conformation, crystallization behavior, electrical and mechanical properties of electrospun polymer-carbon nanotube hybrid nanofibers with different orientations. Carbon. 2012;50:5605–17.
39. Yoshioka T, Dersch R, Tsuji M, Schaper AK. Orientation analysis of individual electrospun PE nanofibers by transmission electron microscopy. Polymer. 2010;51:2383–9.
40. Joziasse CAP, Veenstra H, Grijpma DW, Pennings AJ. On the chain stiffness of poly(1actide)s. Macromol Chem Phys. 1996;197:2219–29.
41. Zhang H, Luo X, Lin X, Lu X, Zhou Y, Tang Y. Polycaprolactone/chitosan blends: simulation and experimental design. Mater Des. 2016;90:396–402.
42. Mattice WL, Helfer CA, Sokolov AP. On the relationship between the characteristic ratio of a finite chain, C_n, and the asymptotic limit, C_∞. Macromolecules. 2003;36:9924–8.
43. Kugler J, Fixher EW, Peuscher M, Eisenbach CD. Small angle neutron scattering studies of poly(ethylene oxide) in the melt. Makromol Chem. 1983;184:2325–34.
44. Bortel E, Hodorowicz S, Lamot R. Relation between crystallinity degree and stability in solid state of high molecular wight poly (ethylene oxide)s. Makromol Chem. 1979;180:2491–8.
45. Saujanya C, Radhakrishnan S. Crystallization behavior of polyethylene oxide/para-nitroaniline microdispersed composites. J Appl Polym Sci. 1997;65:1127–37.
46. Luo H, Huang Y, Wang D, Shi J. Coaxial-electrospinning as a new method to study confined crystallization of polymer. J Polym Sci Polym Phys Ed. 2013;51:376–83.
47. Wang C, Hsieh TC, Cheng YW. Solution-electrospun isotactic polypropylene fibers: processing and microstructure development during stepwise annealing. Macromolecules. 2010;43:9022–9.
48. Strobl GR, Schneider M. Direct evaluation of the electron density correlation function of partially crystalline polymers. J Polym Sci Polym Phys Ed. 1980;18:1343–59.